JOURNAL OF MAGNETIC RESONANCE **127,** 109–114 (1997)
ARTICLE NO. MN971180

Two-Dimensional Rotating-Frame NQR Imaging

H. Robert and D. Pusiol

Facultad de Matemática, Astronomía y Física, Universidad Nacional de Córdoba, Ciudad Universitaria, 5000 Cordova, Argentina

Received December 11, 1996; revised April 10, 1997

A new technique for two-dimensional rotating-frame nuclear-quadrupole-resonance imaging in powder or polycrystalline samples is reported. The bidimensional encoding procedure is based on the irradiation of the object by a sequence of pulsed orthogonal radiofrequency linear gradients. The spatial-density function, together with the spectroscopic information, is directly recorded in Cartesian coordinates. Several variants of the encoding procedure are discussed, and experimental results demonstrating the viability of the technique are given.

INTRODUCTION

It has been demonstrated that one-dimensional projections (or profiles) of polycrystalline solid samples containing quadrupolar nuclei can be recorded using a NQR version (*1–3*) of Hoult's NMR rotating-frame technique (*4*).

One-dimensional NQR spatial encoding (ρNQRI) is based on the application of a radiofrequency amplitude gradient of a single variable-excitation pulse. A 1D spin-density profile is reconstructed from a 2D data matrix, $S(t, t_x)$, which is in turn created by recording the free-induction decay signal as a function of the evolution time t and incrementing the RF pulse length t_x in a stepped manner from experiment to experiment. The resulting nutation spectrum can be considered as a projection of the three-dimensional nuclear spin density onto the axis along which the RF gradient was applied. Thus, the second dimension, ω_1, represents a one-dimensional projection of the object correlated with the spectroscopic information contained in the conventional ω dimension, providing a spatially resolved NQR spectroscopy method (*5*).

Two-dimensional spatial variation—a spin-density cross image—has been obtained from a set of 1D projections which was recorded at different orientations of the RF field-gradient direction relative to the object (*6*). The various linear gradients were generated by means of a single gradient surface coil and a step-by-step rotation of the sample. From a sufficient number of such projections onto different axes, it is possible to partially reconstruct the two-dimensional spin-density function by means of the well-known image reconstruction technique (*7*).

In this paper, a new technique of forming two-dimensional images of a macroscopic sample by means of NQR is reported. The bidimensional rotating-frame imaging technique (2D ρNQRI) is based on the application of a sequence of pulsed orthogonal RF linear gradients to the sample. The spatial spin-density function is then directly reconstructed by a two-dimensional data-evaluation procedure.

One of the important features of the 2D or 3D encoding procedures is the way in which the sample points are distributed (*7, 8*). In the image reconstruction from projections, a polar sampling is applied so that the low-spatial-frequency components are obtained with higher precision than the high-frequency components of the image. Consequently, the coarse features are better represented than the details. The technique described does not involve one-dimensional projections of the object, and the spin-density function is directly measurable in a Cartesian coordinate system. This means that for 2D ρNQRI, high spatial frequencies are reconstructed with the same accuracy as the lower ones, resulting in improved resolution of regions such as edges where the spin density changes rapidly.

TWO-DIMENSIONAL ρNQRI PROCEDURES

Figure 1 shows the RF pulse sequence for 2D spatially resolved NQR spectroscopy. It consists of two pulses which are varied in length. Equivalently, an amplitude-variable pulse scheme can be applied if the irradiation bandwidth must be kept constant during the experiment. Orthogonal RF linear gradients, G_x and G_y, are successively applied for intervals t_x and t_y, and the FID signal is sampled in the third time interval as a function of t. The irradiation sequence is repeated for a full set of equally spaced t_x and t_y values. The 3D signal, $S(t, t_x, t_y)$, contains all the information necessary to reconstruct the set of NQR spectra resolved in the two spatial coordinates, x and y.

The calculations of the quadrupole system response to some variants of the encoding scheme are easily worked out in the quadrupole interaction representation. In this picture, a set of three operators, as defined by Pratt (*9*), form a complete basis set for the ensamble of noninteracting spin-$\frac{3}{2}$ nuclei to describe the effects of RF pulses and free-evolution periods (*10*). For the sake of simplicity, we consider a

1090-7807/97 $25.00

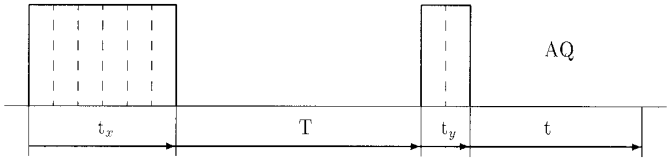

FIG. 1. Pulse scheme for the 2D rotating-frame method. The first preparation pulse is applied with an encoding gradient in the *x* direction and the second encode and read pulse uses a gradient in the *y* direction. In some variants of the encoding procedure, a constant interval *T* of free evolution is included in order to destroy the transverse coherence produced by the first pulse. Both irradiation intervals are incremented step by step in successive experiments to map out the complete *xy* plane.

single resonance line and assume the RF pulses to be strong enough that off-resonance effects during its application can be neglected.

A first variant of the encoding procedure consists of applying the two colinear pulsed fields, H_1 and H_2, successively for intervals t_x and t_y. This means that the separation interval T is in practice negligible in comparison with the transverse relaxation time of the spin system, T_2.

At the end of the two encoding periods, the amplitude of the FID signal depends on both the *x* and *y* coordinates. The resulting expression for the FID signal becomes

$$S(t, t_x, t_y) \sim W(t)F(t_x, t_y), \qquad [1]$$

where

$$W(t) = \int_{-\infty}^{+\infty} d(\Delta\omega)g(\Delta\omega)\cos[(\omega - \Delta\omega)t] \qquad [2]$$

contains the full spectroscopic information, and

$$F(t_x, t_y) = \int_0^{+\infty} dx \int_0^{+\infty} dy H_d \rho(x, y) \int_0^{2\pi} d\phi \int_0^{\pi} d\theta \times \sin\theta\lambda(\theta, \phi)\sin(\omega_1' t_x + \omega_2' t_y).$$

H_d is the magnitude of the RF field generated by the receiver coil. The function $g(\Delta\omega)$ takes into consideration the finite linewidth of the NQR resonance; $\Delta\omega = \omega_0 - \omega$ defines both the offset and the EFG inhomogeneity effects, and $\rho(x, y)$ represents the two-dimensional spin-density function. The orientational dependence of the quadrupole system response is introduced through the function

$$\lambda(\theta, \phi) = (2a\sqrt{3})^{-1} \times \sqrt{(2\eta\cos\theta)^2 + \sin^2\theta(9 + \eta^2 + 6\eta\cos 2\phi)},$$

where the polar and azimuthal angles, θ and ϕ, define the relative orientations of the principal axes of the EFG tensor and the RF field directions, and η is the asymmetry parameter of the EFG tensor. The effective nutation frequencies of the spins, ω_1' and ω_2', are given by the expression $\omega_i' = \lambda(\theta,\phi)\gamma H_i$, for $i = 1, 2$. Here γ denotes the gyromagnetic ratio of the nuclei.

If the gradients, G_x and G_y, are constants and aligned along orthogonal directions, *x* and *y*, a wave vector **k** can be defined

$$\mathbf{k} = (k_x, k_y) = (\gamma G_x t_x, \gamma G_y t_y)\lambda(\theta, \phi). \qquad [3]$$

The visualization of the encoding procedure as a simple trajectory scanning in the **k** plane of Fourier components (*11*) is obtained only in the case of a single crystal. In this particular case, the process of changing the pulse length t_y, for a fixed value of t_x, can be visualized as the sampling of a single line in the **k** plane parallel to the *y* axis. The intercept of this line along the orthogonal axis is changed by increasing the first pulse length t_x so that, if proper sampling parameters are used, the first quadrant of the **k** plane is sampled on a Cartesian raster. Due to the orientational dependence of the magnitude of the **k** vector in Eq. [3], indirect visual interpretation of the spatial encoding procedure (as a picture of trajectories in the **k** plane) is provided for polycrystalline or powders materials.

A second alternative we can consider involves the introduction of a time interval *T* between the pulses. This interval is assumed to be much longer than the transverse relaxation time, but shorter than the spin–lattice relaxation constant T_1, so that the transverse coherences created by the first pulse are destroyed. Providing that $T_1 \gg T_2$, as is usual in our solid-state systems, the observed signal results as in Eq. [1], with $W(t)$ given by Eq. [2] and

$$F(t_x, t_y) \sim \int_0^{\infty} dx \int_0^{\infty} dy H_d \rho(x, y) s_1(t_x) s_2(t_y), \qquad [4]$$

where the definitions

$$s_1(t_x) = \int_0^{2\pi} d\phi_1 \int_0^{\pi} d\theta_1 \sin\theta_1 \cos[\omega_1\lambda(\theta_1, \phi_1)t_x]$$

and

$$s_2(t_y) = \int_0^{2\pi} d\phi_2 \int_0^{\pi} d\theta_2 \sin\theta_2\lambda(\theta_2, \phi_2) \times \sin[\omega_2\lambda(\theta_2, \phi_2)t_y] \qquad [5]$$

were introduced. The parameters ω_i are defined as $\omega_i = \gamma H_i$ $(i = 1, 2)$. For the calculations of this response function, different orientations of H_1 and H_2 with respect to the EFG tensor axis have been assumed.

This second variant has two principal advantages: (*i*) the 2D pseudo-FID, $F(t_x, t_y)$, provides a separable function in

both pseudo-time domains, t_x and t_y, which is more convenient for the image reconstruction procedure from the computational point of view, and (*ii*) when only one transmitter or nondecoupled coils are used, an active detuning method must be implemented, and it is necessary to take account of the unavoidable switching time of the active components.

Whichever method is chosen, we collect FIDs for a set of $N_x \times N_y$ values of t_x and t_y, the number depending on the desired resolution, and the 2D function, $F(t_x, t_y)$, allows one to reconstruct $\rho(x, y)$ as explained in the next section.

In a third variant of the encoding scheme, the second read pulse is replaced by a train of $G_{1,y}$ read pulses, and the signal is acquired in the gaps between the pulses. If the second irradiation pulse is replaced by the rapid rotating-frame pulse sequence (SEXI) (*11*), the complete t_y evolution of the system for each t_x value defined by the first pulse is measured in one experiment. Then, the complete 2D function $F(t_x, t_y)$ is created in just N_x increments of the value of t_x.

The 2D spatial mapping described in this section does not provide distinct cross sections but rather a projection of the 3D spin density onto a two-dimensional plane. A true cross section of a polycrystalline object can be obtained by the previously published slice-selection method (*12*). A zero-crossing magnetic field gradient is applied along the third direction, so that only the slice near the zero-field plane will appreciably contribute to the signal amplitude. The strength and/or shape of the magnetic field will determine the slice thickness.

TWO-DIMENSIONAL IMAGE RECONSTRUCTION

As is well known, the point response function is more complicated for NQR in powders than for NMR, and special data-evaluation procedures must be applied in this case (*13, 14*). The reconstruction procedure must take into consideration both the orientational dependence of the nutation frequency, which results in an inhomogenous broadening of the nutation lineshape, and the departure of the encoding gradients from linearity and orthogonality over the sample volume.

For powder materials, with a random distribution of the EFG tensor axis with respect to the RF field direction, one assumes that each voxel contains all the possible orientations. The orientational distortion of the image, even for an arbitrary value of η, can then be overcome by suitable reconstruction procedures (*14*).

For the reconstruction of the planar images from Eq. [4], we have implemented a true 2D version of the maximum-entropy method (MEM). The extension of the one-dimensional maximum-entropy procedure is straightforward and was previously described for 2D NMR spectroscopy (*15, 16*).

Briefly, 2D MEM consists of finding the real and positive spectrum, $X(\omega_1, \omega_2)$, which both maximizes an entropy $H(X)$ and is consistent with the observed time-domain data, $F(t_x, t_y)$. In the case of 2D ρNQRI, the transformation between the pseudo-time and frequency domains becomes

$$F(t_x, t_y) = \int_0^\infty \int_0^\infty d\omega_1 d\omega_2 X(\omega_1, \omega_2) R(t_x, \omega_1, t_y, \omega_2).$$

R is the transfer matrix of the quadrupole system, given by

$$R(t_x, \omega_1, t_y, \omega_2) = s_1(t_x) s_2(t_y),$$

where $s_1(t_x)$ and $s_2(t_y)$ are given by Eq. [5].

As the entropy $H(X)$ of the spectrum is independent of the organization of the intensities, it can be written

$$H(X) = \int_0^\infty \int_0^\infty d\omega_1 d\omega_2 \frac{X(\omega_1, \omega_2)}{A} \ln\left(\frac{X(\omega_1, \omega_2)}{A}\right),$$

where the background parameter, A, can be regarded as the default level for the spectral intensities, X. The consistency constraint is expressed in terms of the least-squares parameter, χ^2. The problem to be solved by MEM is then to find the 2D spectrum X that maximizes the entropy, H, subject to the constraint χ^2 equal to the number of data points.

Finally, the desired spatial distribution is obtained from $X(\omega_1, \omega_2)$ by the relation

$$\rho(x, y) = \frac{1}{H_d} \left| \frac{d\omega_1(x)}{dx} \right| \left| \frac{d\omega_1(y)}{dy} \right| X[\omega_1(x), \omega_2(y)],$$

which takes into account the coordinate transformation between the frequency and spatial domains.

After removing the powder distribution from the 2D nutation NQR spectrum, $X(\omega_1, \omega_2)$, the surfaces of constant H_i correspond to surfaces of constant nutation frequency $\omega_i = \gamma H_i$, and the total NQR intensity in each frequency interval is proportional to the number of nuclei in the sample lying between those surfaces.

It should be noted that with NQR, the magnitude of the RF coil magnetic field at any position is relevant for the spin excitation and detection, whereas in the NMR case, only the components transverse to the external magnetic field must be considered. In order to keep image reconstruction simple, the surfaces of constant field should ideally be planes perpendicular to the gradient directions, and the RF encoding gradients, G_x and G_y, must be orthogonal everywhere over the sample volume.

In order to estimate the deviation from linearity and orthogonality of the gradients in a real situation, we have calculated the magnetic field distribution for the circular and rectangular coil geometries used in this work. Figure 2a is a contour presentation of the magnetic field intensity (magnitude) for the circular surface coil of 1 cm radius lying in

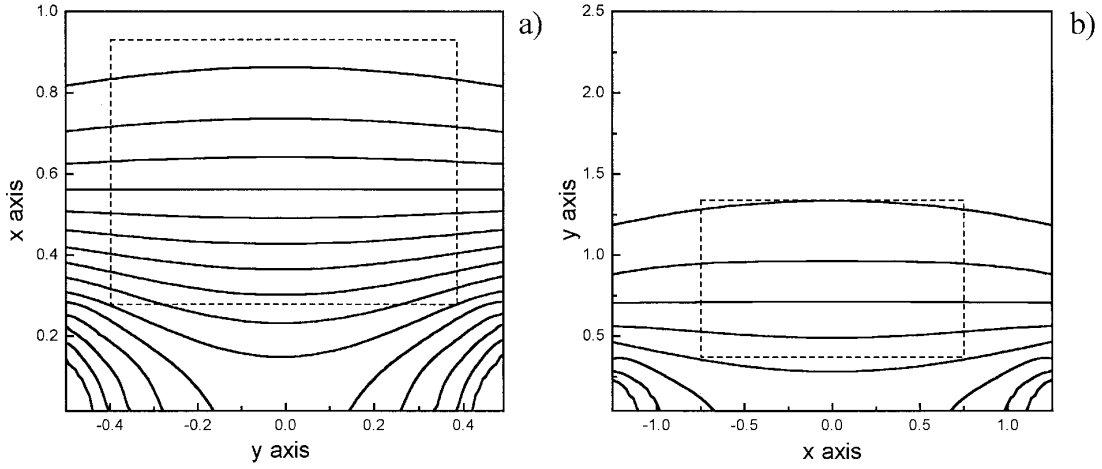

FIG. 2. Calculated RF field magnitude map in the *xy* plane for a flat circular (a) and rectangular (b) coils, lying in the *yz* and *xz* planes, respectively. The dashed rectangles indicate the convenient regions for rotating-frame experiments.

the *yz* plane (the coil depth axis is the *x* axis). It is shown that in the range of relative distance $|y| < 0.5$ from the coil axis, the field profile is reasonably homogeneous; i.e., the modulus of the magnetic field is almost independent of *y* and drops off linearly with *x* in the range $0.2 < x < 1$. Figure 2b shows the computed magnetic field distribution for a rectangular coil 3 cm long and 1.5 cm wide. The contour plot indicates that a convenient region for rotating-frame experiments is the range $|x| < 1$ and $0.25 < y < 1.25$, where the RF magnitude is nearly independent of *x* and has a gradient in the *y* direction.

The sample can be positioned in the region indicated by the dashed rectangles so that the curvature of the surfaces of constant field can simply be neglected, because the spatial distortion over the whole dimensions of the objects will be less than the pixel resolution.

In practice, it is not possible to entirely prevent current being induced between the adjacent transmitter coils so that unpredictable changes to the profiles of such calculated fields are expected. Thus, gradient calibrations should be carried out using test objects.

PROBEHEAD AND NQR SPECTROMETER

The 2D experiments were carried out on a homebuilt NQR spectrometer (*11, 12*) equipped with a dedicated probe. Figure 3a shows the means by which two orthogonal RF field gradients were provided. Two surface coils were built into a single probe using the tuning and matching capacitors to fulfill the resonant and matching conditions. The probe includes a circular surface coil of 22 mm diameter, delivering the *y* gradient and used for signal detection, and positioned with respect to the rectangular coil as Fig. 3a shows. The rectangular coil, 30×15 mm, generates the second *x* gradient.

In order to diminish the coupling between the resonant circuits and to select the transmitter coil, we implemented the circuit proposed by Bendall *et al.* (*17*) to actively tune and detune the adjacent RF coils. The resonant circuits were connected to the same RF power amplifier, and each coil was connected to ground through a $\lambda/4$ cable. An active means to quickly insert (<1 ms) a high/low impedance point into the circuit was provided by reed-relays at the ends of the $\lambda/4$ cables. The resonant circuits can then be used independently by closing one of the two relays.

EXPERIMENTS

To demonstrate the feasibility of 2D ρNQRI, the third variant of the encoding procedures described above was implemented.

The NQR phantom used in the first experiment consists of three cylindrical layers of paradichlorobenzene powder, 12 mm in diameter and 3 mm thick. PTF spacers were inserted between the layers, and the sample was positioned in the best constant-gradient region of the coil arrangement as is shown in Fig. 3a.

The number of samples selected was 64 in the t_y dimension, and a set of 48 pseudo-FIDs was recorded for the t_x pulse widths starting at 10 μs with increments of 10 μs. The separation pulse interval *T* was 3 ms. The total time required for one complete experiment was about 8 minutes, with 10 transients per pseudo-FID and a repetition time of 1 s.

From the set of pseudo-FIDs, the 2D image of Fig. 3b was reconstructed on a 128×128 matrix by the two-dimensional MEM procedure. Although the final image does not exactly reproduce the original structure of the object, due to the nonlineality of the RF gradients, the result demonstrates the feasibility of the proposed method.

A second experiment was performed with the same coil

arrangement and identical parameters. The cross section of the original object is shown in Fig. 4a. The final image of Fig. 4b was reconstructed by MEM on a matrix of 128 × 128. Adequate RF field corrections were implemented to compensate for the spatial sensitivity dependence of the receiver coil. Additionally, the image coordinates have been corrected for the nonlineality of the RF gradients.

DISCUSSION

The 2D ρNQR imaging technique described in this work allows one to map the two-dimensional quadrupolar nuclei distribution without rotation of the object and with improved edge resolution. The described encoding procedures permits the recording of 2D spatially resolved spectroscopic information. As no rotation of the object and/or mechanical contact with the sample by any external device are involved, these techniques are particularly suitable for the detection of the bidimensional spatial distribution of physical parameters influencing the NQR spectrum. A variant has been presented to speed up data acquisition when the spectroscopic information can be disregarded. It should be possible to improve the images by paying attention to the linearity of the RF field gradients. In this respect, further improvements of the technique will require better design of the surface coil arrangement.

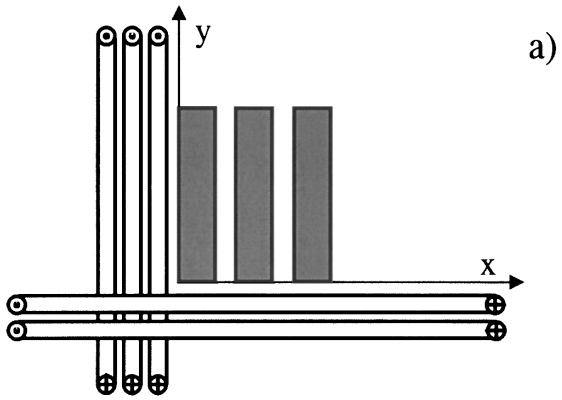

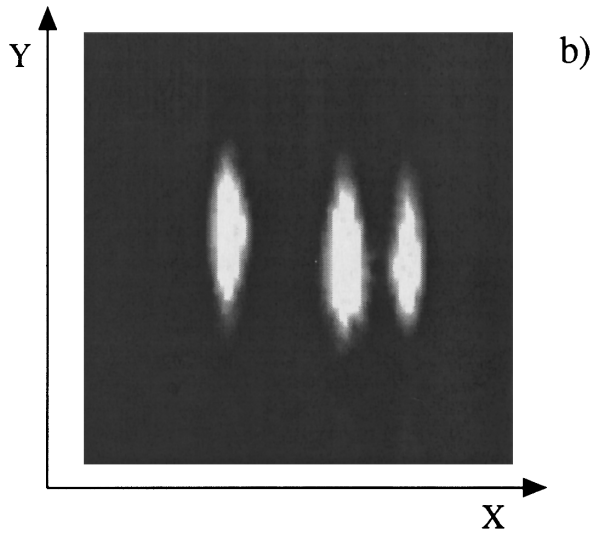

FIG. 3. (a) Schematic representation of the two-coil arrangement and geometrical structure of the test object. The dimensions of the layers were 10 mm diameter and 3 mm thick. (b) MEM's reconstructed bidimensional image of the powder phantom.

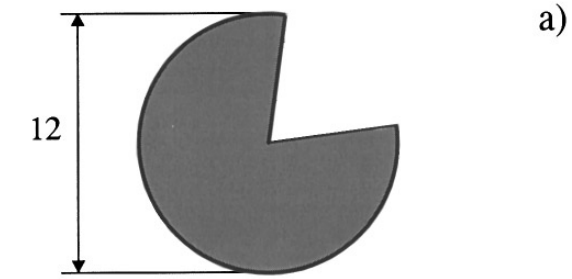

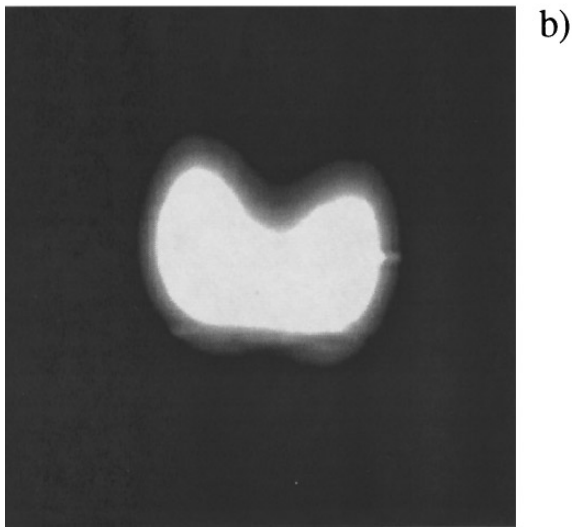

FIG. 4. (a) Representation of the cross section of the second test object and (b) two-dimensional image reconstructed by MEM from a set of 48 × 64 pseudo-FIDs.

ACKNOWLEDGMENTS

The authors thank the National and Provincial Research Councils (CONICET and CONICOR, respectively), as well as the Fundación Antorchas of Argentina. H.R. thanks CONICET for a Research Fellowship. This work is part of the Ph.D. Thesis of H.R.

REFERENCES

1. E. Rommel, P. Nickel, R. Kimmich, and D. Pusiol, *J. Magn. Reson.* **91,** 630 (1990).

2. E. Rommel, D. Pusiol, P. Nickel, and R. Kimmich, *Meas. Sci. Technol.* **2,** 866 (1991).
3. R. Kimmich, E. Rommel, P. Nickel, and D. Pusiol, *Z. Naturforsch. A* **47,** 361 (1992).
4. D. I. Hoult, *J. Magn. Reson.* **33,** 183 (1979).
5. P. Nickel, H. Robert, R. Kimmich, and D. Pusiol, *J. Magn. Reson. A* **111,** 191 (1994).
6. P. Nickel, E. Rommel, R. Kimmich, and D. Pusiol, *Chem. Phys. Lett.* **183,** 183 (1991).
7. P. G. Morris, ''Nuclear Magnetic Resonance Imaging in Medicine and Biology,'' Clarendon Press, Oxford, 1986.
8. P. T. Callaghan, ''Principles of Nuclear Magnetic Resonance Microscopy,'' Clarendon Press, Oxford, 1991.
9. J. C. Pratt, *Mol. Phys.* **34,** 539 (1977).
10. H. Robert, A. Minuzzi, and D. Pusiol, *J. Magn. Reson. A* **118,** 189 (1996).
11. Stig Ljunggren, *J. Magn. Reson.* **54,** 338 (1983).
12. H. Robert and D. Pusiol, *J. Magn. Reson. A* **118,** 279 (1996).
13. E. Rommel, R. Kimmich, H. Robert, and D. Pusiol, *Meas. Sci. Technol.* **3,** 446 (1992).
14. H. Robert, D. Pusiol, E. Rommel, and R. Kimmich, *Z. Naturforsch. A* **49,** 35 (1994).
15. P. J. Hore, *J. Magn. Reson.* **62,** 561 (1985).
16. E. D. Laue, M. R. Mayger, J. Skilling, and J. Stauton, *J. Magn. Reson.* **68,** 14 (1986).
17. M. R. Bendall, J. McKendry, I. Cresshull, and R. Ordidge, *J. Magn. Reson.* **60,** 473 (1984).